Desalination 520 (2021) 115334

Contents lists available at ScienceDirect

Desalination

journal homepage: www.elsevier.com/locate/desal

Molecular layer deposition for the fabrication of desalination membranes with tunable metrics

Brian C. Welch [a,b,*], Olivia M. McIntee [a,b], Tyler J. Myers [c], Alan R. Greenberg [a,b], Victor M. Bright [a], Steven M. George [c]

[a] Department of Mechanical Engineering, University of Colorado, Boulder, CO 80309, USA
[b] Membrane Science, Engineering and Technology Center, University of Colorado, Boulder, CO 80309, USA
[c] Department of Chemistry, University of Colorado, Boulder, CO 80309, USA

HIGHLIGHTS

- MLD added an ultrathin MPD-TMC polyamide active layer to commercial NF membranes.
- Progressive MLD systematically altered flux/rejection metrics from NF to RO values.
- Controlled increase of MLD layer thickness increased rejection but decreased flux.
- Atomic force microscopy revealed that MLD removed small-scale roughness features.

GRAPHICAL ABSTRACT

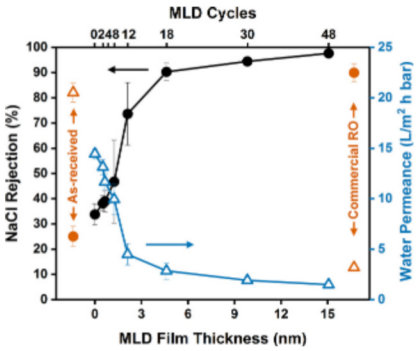

ARTICLE INFO

Keywords:
Molecular layer deposition (MLD)
Thin-film composite (TFC)
Surface modification
RO polyamide membrane
m-Phenylenediamine and trimesoyl chloride

ABSTRACT

The recent advancement of semiconductor devices to the near-atomic scale necessitated the development of atomic layer processing methods, including molecular layer deposition (MLD). This gas-phase deposition technique creates semipermeable polymer films with precise control of composition and thickness. Herein, MLD was used to produce thin-film composite reverse osmosis membranes. Aromatic polyamide films as thin as 0.5 nm were applied to NF270 nanofiltration membranes using *m*-phenylenediamine and trimesoyl chloride. Within two molecular layers, desalination performance was affected. As film thickness increased to 15 nm (48 MLD cycles), performance progressed from nanofiltration to reverse osmosis metrics in terms of salt rejection and water permeance. With film thickness > 5 nm, rejection values exceeded a small sampling of commercial membranes. In all cases, a tradeoff between rejection and permeance was observed. Atomic force microscopy measurements indicate that MLD enhancement led to removal of small-scale roughness features and resulted in a root mean square roughness difference of <0.1 nm from the substrate. These initial MLD studies represent a novel processing approach that offers a potential pathway for the fabrication of membranes with finely tailored properties.

* Corresponding author at: Dept. of Chemistry, Campus Box 215, Boulder, CO 80309, USA.
E-mail addresses: bwelch@colorado.edu (B.C. Welch), olivia.mcintee@colorado.edu (O.M. McIntee), tyler.j.myers@colorado.edu (T.J. Myers), alan.greenberg@colorado.edu (A.R. Greenberg), victor.bright@colorado.edu (V.M. Bright), steven.george@colorado.edu (S.M. George).

https://doi.org/10.1016/j.desal.2021.115334
Received 20 May 2021; Received in revised form 16 August 2021; Accepted 31 August 2021
Available online 21 September 2021

1. Introduction

Conventional thin-film composite (TFC) reverse osmosis (RO) membranes made with interfacial polymerization (IP) require control over a number of important processing parameters. Variations in concentration [1,2], substrate [3–5], solvent [6] and synthesis procedure [7] impact the density, morphology, homogeneity, and thickness of the IP polyamide layer [8]. Such variability in turn can affect desalination performance, operation lifetime and fouling characteristics. While many aspects of the nanometer-scale mechanics of the solution-based film growth have been characterized, its complex nature prohibits comprehensive understanding and control over this decades-old technique [7]. As a result, current methods lean on empirical approaches rather than molecular-level design [2].

Despite these challenges, advances in fabrication have enabled the creation of RO membranes which incorporate ultrathin, chemically and morphologically controlled polyamide active layers. Such characteristics are desirable for minimal transport resistance and improved antifouling behavior [8–10]. The molecular layer-by-layer (mLbL) method [11–16] has proven effective in generating RO membranes with a dense layer as thin as 4 nm and with a root mean square (RMS) roughness of ~1 nm [16]. Free standing film growth techniques have been leveraged to create RO polyamide film thicknesses below 10 nm [1,5,9]. Electrospray processes have also been used to fabricate polyamide RO films as thin as 20 nm and with a RMS roughness that is indistinguishable from the substrate [17]. These complex procedures reiterate the challenge of controlling the liquid phase chemistry at a nanometer scale. While achieving impressive thickness/roughness dimensions, each of these fabrication routes still faces the limitations of IP including incomplete crosslinking and limited consistency in film thickness and density. Additionally, the mLbL and free standing film techniques are difficult to scale up for commercial production and produce films which are prone to delamination, relying on physical adhesion or interlayer materials which are susceptible at extreme pH and salt concentration [14,15,18]. Thus, the need remains for a scalable and robust TFC membrane synthesis technique that enables fine control of film nanostructure and thickness.

Molecular layer deposition (MLD) is a scalable, polymer thin-film deposition technique that can provide extremely thin, smooth, chemically consistent films with nanometer precision [19]. The MLD process is analogous to atomic layer deposition (ALD), differing by its use of organic precursors to incorporate molecular fragments [20]. Whereas ALD precursors typically contribute one atom into a metal or ceramic film, MLD precursors incorporate an entire organic linkage. These techniques have become instrumental in achieving nanoscale transistors and enabling previously unachievable length scales for gate oxides and other components of integrated circuits and memory devices [21,22]. They have also been used in energy storage [23,24] and conversion [25]. ALD and MLD offer exciting possibilities for improved membrane materials and have already been utilized for tuning pore sizes as well as affecting hydrophilicity and fouling characteristics [26].

A schematic of the MLD process is shown in Fig. 1. All-organic MLD is performed under vacuum conditions by introducing a substrate to two gas-phase organic precursors in an isolated and sequential order. Upon exposure to the initial reactant, functional groups of the precursor (e.g. acyl chlorides) react with the functional groups of the surface (e.g. amines). A layer of monomers is added to the surface by a single step of step-growth polymerization. The substrate is now terminated with a new functional end group (acyl chlorides). The precursors are chosen such that self-polymerization will not occur, ensuring self-limited growth at each exposure. Once the reaction environment is cleared of the first precursor and reaction byproducts, the surface is exposed to a second precursor with functional groups which are reactive with those of the first precursor (e.g. amines). The polymer chain-ends are again extended by one monomer in a self-limiting fashion. The reaction space is once again purged. This two-step process constitutes one MLD cycle which may be repeated for controlled growth of polymer films [20]. The formation of polymer films containing crosslinks may be achieved by use of a trifunctional precursor [27]. This sequence of self-limited, step-wise surface saturation provides many advantages. Film thickness is highly controlled, scaling linearly with increasing cycles. Films are smooth and conformal to the substrate surface [28].

MLD is capable of producing semipermeable polymer films for water purification without the use of environmentally harmful solvents; this

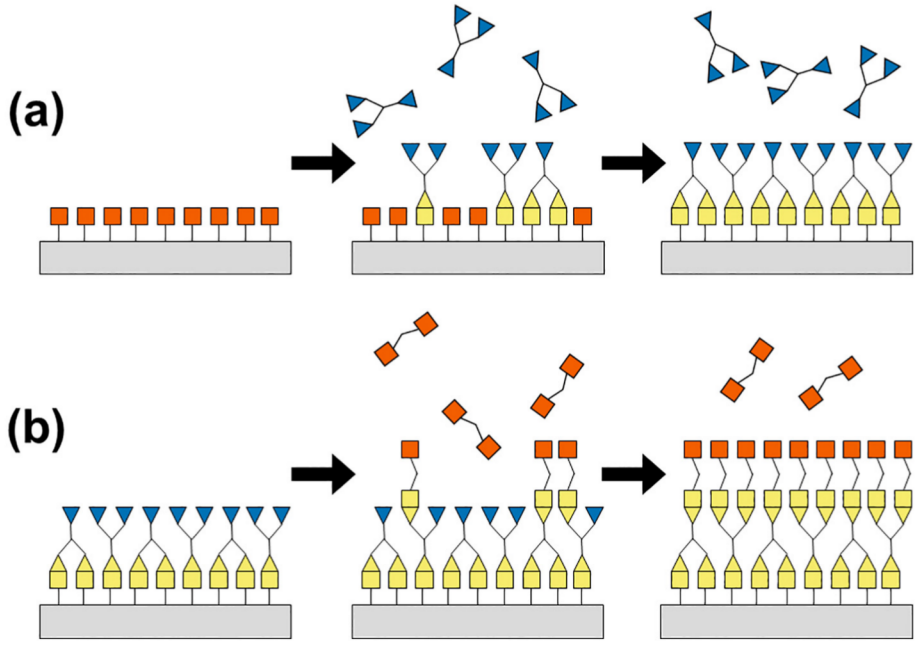

Fig. 1. Schematic of the MLD process. (a) Functional groups on the surface (squares) are exposed to a gas-phase precursor; functional groups of this precursor react with only the surface, forming a single deposited layer. (b) The reaction space is purged and the new surface functional groups (triangles) are exposed to a second gas-phase precursor; the second precursor forms another, self-limited layer. The stepwise process is repeated for desired film thickness.
Adapted from [29].

includes the often-used aromatic polyamide made from *m*-phenylenediamine (MPD) and trimesoyl chloride (TMC) [30–32]. Homogenous films grown with this controlled, layer-by-layer technique are ideal in view of recent work by Culp et al. which concluded that membrane resistance is the result of nanoscale variations in thickness and density [8].

In principle, MLD is very much akin to the mLbL technique: both are layer-by-layer processes which grow polymer films with monomer precision. Each method creates smooth, conformal films, but each has its own advantages. MLD exhibits more control over film thickness with a deposition rate around 0.4 nm/cycle compared to the mLbL rate of ~1 nm/cycle [13,30]. The liquid phase mLbL may be done at ambient temperatures but requires heavy solvent usage and long cycle times. The mLbL solution chemistry is simple to perform on the lab bench but is difficult to scale for commercial production. Gas-phase MLD requires temperatures sufficient to vaporize the reactants, but the solvent-free technique can be performed with sub-second cycles times [30]. MLD is compatible with commercial scale roll-to-roll (R2R) processing and has a clear path to manufacture [33,34]. Despite its advantages, fabrication of a robust, freestanding MLD film remains a difficult objective due to the conformal, isotropic manner of film growth. MLD precursors diffuse into pore openings and deposit material within, not across pore openings [32]. Thus, fabrication of desalination membranes using MLD has been a significant technical challenge.

This paper demonstrates that the advantages of MLD can be realized by utilizing nanofiltration (NF) TFC membranes as a suitable substrate. The existing films atop NF membranes provide sufficient transport resistance to MLD precursors which would otherwise deposit onto pore walls. FilmTec NF270 membranes were chosen as the substrate for subsequent MLD processing given their ability to withstand high temperature exposure in a vacuum. This study explores the ability to control the tradeoff between salt rejection and water permeance by altering the MLD film thickness. To the authors' knowledge, this study represents the first demonstration of active membrane films made by gas-phase MLD.

2. Materials and methods

2.1. Membrane materials

This work primarily utilized NF270 nanofiltration membranes which were kindly provided by DuPont Filmtec. The support layer of this TFC membrane is polysulfone (40 μm thick) on a non-woven polyester backing (120 μm thick) [35]. Polysulfone has a glass transition temperature of 190-230 °C [36]. The active layer is a semi-aromatic polyamide (270 nm thick) made via interfacial polymerization of piperazine and TMC [37–40]. As indicated by the manufacturer, the maximum operating temperature is 45 °C [41].

Limited testing was also conducted using HYDRACoRe50 nanofiltration membranes generously provided by Nitto Hydranautics. This membrane has an active layer comprised of sulfonated polyethersulfone with a molecular weight cutoff of 1 kDa and a maximum operating temperature of 45 °C [42].

Performance metrics for several commercial RO membranes were used in this study to provide a basis for comparison, and the relevant information is detailed in Table 1.

2.2. Preconditioning of the membranes

To precondition the samples, membranes were soaked in a 20% isopropanol solution for at least 30 min, then rinsed with ultrapure water (Milli-Q® Advantage A10, MilliporeSigma). "As-received" samples were then measured in a dead-end cell with no further handling. MLD-modified samples were dried at ambient conditions prior to being placed in the MLD vacuum chamber. Before desalination testing, the processed samples were rewet with a 50% ethanol solution for at least 15 min to reopen the pores [43]. After soaking, these membranes were rinsed with ultrapure water and kept wet until the measurements were completed.

2.3. Spatial molecular layer deposition reactor

A custom built, spatial MLD system was utilized to deposit polyamide thin films on the NF membrane substrates. The MLD reactor is a cylinder-shaped vacuum chamber made of outer and inner drums placed concentrically with a 1 mm gap (Fig. 2). Samples are mounted to the inner drum which is able to rotate about a shaft. Two reactive gas-phase precursors are fed into to the outer drum at opposite ends to create isolated reaction zones. The MLD sequence is performed by rotating the inner drum so that the samples move from one reaction zone to the other. Reaction-free zones exist in between the reaction zones to provide purging times between each exposure. More details on the design [30,47] and operation [31,32,48,49] of this system are described elsewhere.

An aromatic polyamide material was formed with MPD (99%, Sigma Aldrich) and TMC (98%, Sigma Aldrich). These precursors were dosed at flowrates which produced 2.7×10^{-4} bar (200 mTorr) of pressure above the base pressure of 4.8×10^{-4} bar (360 mTorr). System pressure was monitored with capacitance monometers (121A Baratron®, MKS); one at each dosing line and the third at the drum volume. A flow of nitrogen (4.8 grade, Airgas) on either side of each dosing zone served as a diffusion barrier to confine the reactants. Total nitrogen flow was 100 standard cm^3/min.

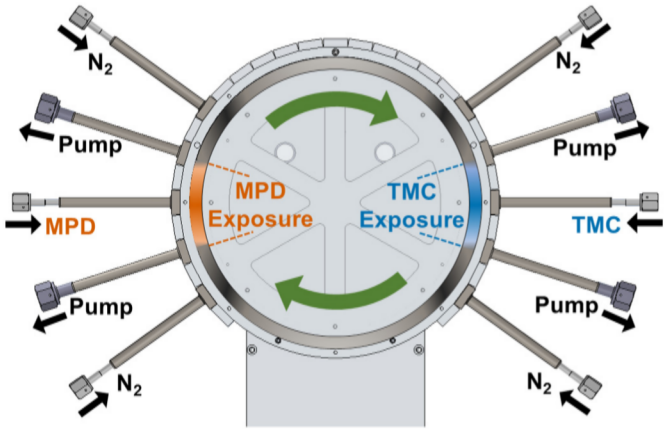

Fig. 2. Cross-sectional diagram of the spatial MLD reactor.

Table 1
Desalination performance metrics for various commercially available flat sheet membranes. Values were obtained from the manufacturers' data sheets.

Membrane product	Type	Manufacturer	Permeate flow rate GFD (L/m^2 h)	Salt (NaCl) rejection (%)	Test pressure bar (psi)	Source
NF270	NF	DuPont Filmtec	51.8 (30.5)	40-60 ($CaCl_2$)	4.8 (70)	[41]
HYDRACoRe50	NF	Nitto Hydranautics	73.0 (43.0)	55	9.7 (140)	[42]
TMG(D)	RO	Toray	51.3 (30.2)	99.7	10.3 (150)	[44]
BW30LE	RO	DuPont Filmtec	48.8 (28.8)	99.3	10.3 (150)	[45]
AG	RO	Suez	44 (26)	99.5	15.5 (225)	[46]

Membrane samples were mounted onto the inner drum of the reactor using Kapton tape with acrylic adhesive. All edges were sealed with the adhesive tape to prevent backside deposition. A silicon coupon was adhered to the drum beside each membrane sample to serve as a "witness" to film growth. Film thickness was measured on the silicon coupons using spectroscopic ellipsometry.

The MLD system was slowly heated within a custom-built convection oven. The system took 5 h to heat to 115 °C. Reactions were performed after an additional 6 h to ensure thermal equilibrium within the vacuum chamber. Thus, total heating time was 11 ± 1 h to achieve a system temperature of 115 °C. Following the reaction, heaters were then turned off while the convection fan continued running to ensure slow, controlled cooling.

Drum rotation speed was controlled by a stepper motor (MDrive23Plus, Schneider Electric). A slower rotation speed corresponded to increased dosing and purging times. The samples were exposed to precursors while rotating through the region between the pumping modules. Each dose had an exposure time in seconds equal to $6/\omega$, where ω is the rotation speed in RPM. Purge times in seconds were equal to $24/\omega$.

Before each reaction, dosing lines were opened over a blank position on the inner drum, one at a time until pressures reached a steady state. This allowed for constant flow rates during the reaction and a purge of any impurities with higher vapor pressures. Once steady state was individually achieved in the precursor lines, both lines were opened simultaneously. At this point, the inner drum was accelerated from a standstill to the specified rotation speed at a rate of ~20 RPM/s. The drum was decelerated to stop at the specified number of rotations. A constant rate of rotation was otherwise maintained. Once the inner drum rotation was complete, dosing lines were closed and subjected to a purging procedure.

2.4. Spectroscopic ellipsometry

The thickness of the deposited polyamide films was measured with spectroscopic ellipsometry (M-2000, J.A. Woollam Co., Inc.). As previously noted, MLD films were grown on witness silicon coupons which were located next to the membrane samples.

2.5. Dead-end desalination measurements

Desalination tests of the membrane samples were performed in a stirred, dead-end cell (HP4750, Sterlitech). Membrane samples had an effective area of 11.8 cm^2. The feed solution had a volume of 287 mL and a concentration of 2000 ± 10 ppm NaCl. The cell was pressurized with nitrogen to a pressure of 15.5 bar (225 psig) at 22 °C. Membranes with a permeance less than 5 L/m^2 h bar were pre-compressed in the cell with the salt solution at 15.5 bar (225 psig) until 200 g of permeate was captured; the limit of the cell volume made precompression of the more permeable membranes impractical. Salt concentration was measured with a conductivity probe with a cell constant of 0.621 ± 0.1 (FP30, Mettler Toledo). A temperature coefficient value of 2.14%/K was used as well as total dissolved solids conversion factor which was interpolated from the technical manual of the probe [50]. The permeate was collected in a cumulative fashion and measured using the gravimetric method. Apparent salt rejection (R) and water permeance (A_s) were calculated according to Eqs. (1) and (2), respectively [51]:

$$R = 1 - c_p/c_f \tag{1}$$

$$\mathrm{A_s} = \frac{\Delta V}{\Delta t \bullet s \bullet}(\Delta p - \Delta \Pi) \tag{2}$$

Here, c_p is the concentration of the cumulative permeate, c_f is the concentration of the initial salt solution, s is the membrane area, Δp is the transmembrane pressure and ΔV is the change in volume over the time span, Δt. The difference in upstream and downstream osmotic pressure, $\Delta \Pi$ was calculated using the Van't Hoff relationship with an osmotic constant of 0.92 [52]. Calculation of average salt rejection and water permeance was taken over the span of 40 to 50 g of collected permeate. Each measurement was done in triplicate except in a few cases where samples ruptured or measurement failed. Error bars were calculated to represent the standard deviation from the mean.

2.6. Cross flow desalination measurements

Membranes were tested in a 2.6 × 7.7 cm cross flow cell. The channel height was 0.3 cm and cross flow velocity was 0.19 ± 0.02 m/s. Membranes were pre-compressed at 17.2 bar (250 psi) for at least 15 h. Pure water flux was then measured at 15.5 bar (225 psi) using the gravimetric method. Desalination tests were performed with a feed solution of 2000 ppm NaCl at 15.5 bar (225 psi). Temperature was maintained at 26 °C. Permeate flux was measured using the gravimetric method and the salinity of the feed and permeate was monitored with the conductivity probe.

2.7. Contact angle measurements

Contact angle measurements were performed on membrane surfaces with the Theta Lite system (Biolin Scientific). Images were processed using OneAttension (Biolin Scientific). Measurements were done in triplicate with error bars representing the standard deviation from the mean.

2.8. Atomic force microscopy

Atomic force microscopy (AFM) measurements were performed using a Nanosurf EasyScan 2. The scanner was fitted with a 10 μm head and Aspire CT170R tips were used as probes. The AFM was operated in tapping mode and acquired 1 μm × 1 μm images at 1 line/s and 256 pixels/line. Raw AFM data were processed and analyzed using Gwyddion [53].

3. Results and discussion

3.1. Molecular layer deposition growth characteristics

Semipermeable aromatic polyamide films were grown with the MLD technique in the spatial reactor. The exposure time was controlled by changing the rotation speed of the drum. The samples were processed at constant rotation speeds. The rotation speeds and corresponding exposure times and purging times are specified in Table 2.

For the same rotation speed, film growth was reasonably linear with increasing cycles (Fig. 3). Films produced with an exposure time of 6 s grew at an average rate of 0.53 nm/cycle whereas films grown with exposure times of 1.2 s or less had an average rate of 0.30 nm/cycle.

The increased growth rate at longer exposure times is attributed to absorption effects. The TMC and MPD vapors enter the bulk structure of polymer substrates by the solution-diffusion mechanism [54]. Longer exposure times result in greater concentration levels of the absorbed reactant within the substrate. For a 6 s exposure, it appears that a purge time greater than 24 s is necessary to fully desorb the precursors. If purging time is insufficient, absorbed monomers may be carried into the subsequent exposure zone and react with the other precursor at the surface. This would lead to an increased growth rate per cycle. This

Table 2
Exposure and purging times corresponding a given drum rotation speed in the spatial MLD reactor.

Rotation speed (RPM)	Exposure time (s)	Purging time (s)
20	0.3	1.2
5	1.2	4.8
1	6	24

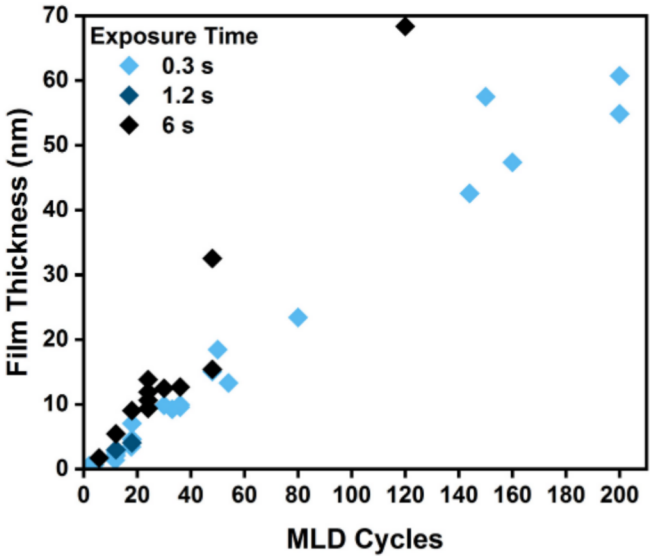

Fig. 3. Thickness of MLD films with increasing cycles, measured from silicon coupons with spectroscopic ellipsometry. Films were grown with TMC and MPD precursors at 115 °C in the spatial reactor.

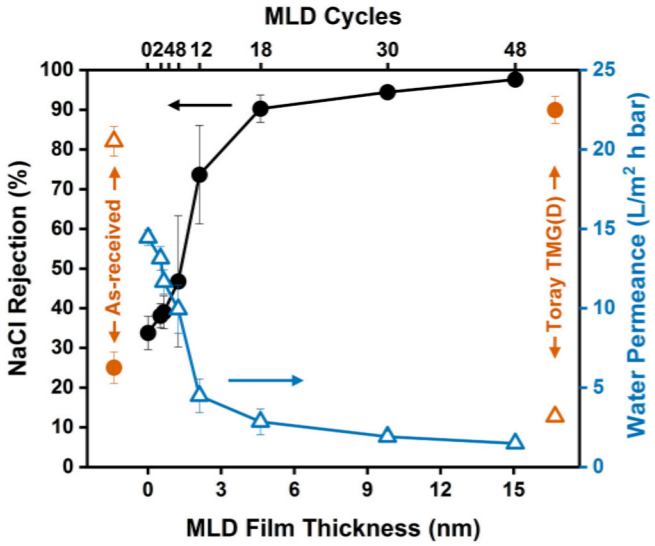

Fig. 4. Desalination performance of NF270 membranes topped with increasing MLD film thickness. MLD was processed in a spatial drum reactor with a 0.3 s exposure at 115 °C with TMC and MPD precursors. The 0-cycles data point represents samples placed in the MLD vacuum chamber with no chemistry. Heating times were 11 ± 1 h. Results are compared to the performance of as-received NF270 samples and Toray TMG(D) RO membranes measured using the same dead-end cell procedure.

carry-over phenomenon may occur even with non-absorbing surfaces such as silicon as they become coated with the absorbing MLD polymer. Due to the constant rate of rotation, a change in purging times would require variable rotation speed or a reconfiguration of the reactor geometry.

NF membranes were chosen as the test substrate for MLD modification to take advantage of the existing dense layer which provides a barrier to pore penetration by MLD precursors. The MLD precursors attach to the NF membrane covalently through reactions with functional groups at the membrane surface. In the case of polyamide-topped TFCs such as NF270, the precursors may react with terminal carboxyl and amine groups.

3.2. Desalination performance of modified NF270 membranes

NF270 nanofiltration membranes which were modified via MLD resulted in increased salt rejection with an expected tradeoff of decreased water permeance. Fig. 4 displays the results and compares the MLD data to the performance of an as-received NF270 membrane as well as a commercial RO membrane (TMG(D), Toray). NaCl rejection and water permeance evidenced a non-linear response to an increasing number of MLD cycles processed at 115 °C with a 0.3 s exposure time. This observed empirical inverse correlation between rejection and permeance has been widely reported for polymeric RO membranes as well as for gas separation membranes [55]. Similar thickness-dependent tradeoffs are described for RO membranes made with the mLbL technique [16].

For NF270 membranes processed with 2 - 18 MLD cycles, the initial rejection and permeance could be controllably tuned between NF and RO levels of performance. This suggests that the selectivity for various multivalent salts could also be precisely targeted while maximizing water flux [56]. At 18 MLD cycles (5 nm), the modified NF270 membranes had salt rejection and water permeance performance equal to the commercial RO membrane.

As shown in Fig. 4, a rapid change in rejection-permeance tradeoff was experienced in the first few MLD cycles (< 12 cycles, < 2 nm) whereas the change in metrics was more incremental after 18 cycles (> 5 nm). It is possible to explain this difference as due to a nucleation period. ALD film growth is known to undergo a nucleation period whereby a continuous film is not achieved until several cycles have been performed [57]. Although MLD nucleation is less well understood [19], it may be the case that a complete, fully networked MLD film is not formed atop the NF270 surface within the first 12 cycles. Under this assertion, the first 12 cycles successively approach a complete, networked polymer layer. Each increasing cycle therefore yields marked improvement in NaCl rejection as the top layer is progressively formed. Once the MLD film is fully formed (presumably by 18 MLD cycles), only small gains in the rejection metric are obtained with subsequent cycles, attributed to increasing film thickness.

The rejection-permeance tradeoff is again shown in Fig. 5 which displays the cumulative summary of initial desalination performance for all modified NF270 membranes processed at 115 °C. The initial desalination performance metrics are compared to a small sample of commercial flat sheet membranes measured in the same dead-end cell. With

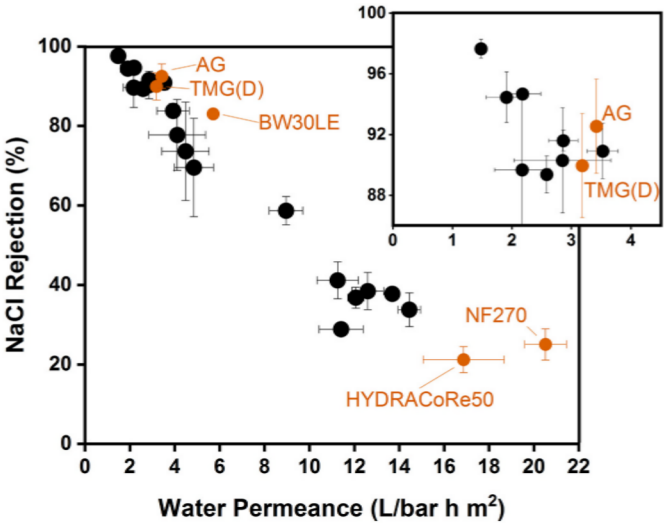

Fig. 5. Cumulative desalination performance for all NF270 membranes modified with MLD. A small sample of commercial desalination membranes are included for comparison. The inset is a magnified view of the data with the highest values of NaCl rejection.

more MLD cycles and increased reactant exposure times, the maximum salt rejection values of the MLD-modified NF270 membranes exceeded those of the unmodified commercial products. While these initial results are encouraging, they should be interpreted cautiously in view of the small sampling of commercial RO membranes and the dead-end test procedure utilized, with the latter likely contributing to the differences between the measured salt rejection values and those listed in Table 1. These results should be viewed in the context of recent studies which indicate that the economics of water purification appear more sensitive to improvements in selectivity behavior rather than flux properties [2,58–60]. Thus, MLD enhancement might be particularly effective for high purity applications which have not been sufficiently served by IP membranes.

To further quantify desalination results, cross flow desalination measurements were performed. The results of the cross flow tests (Fig. S1) were in reasonable agreement with those of the dead-end cell tests as the rejection-permeance tradeoff progressed between NF270 samples topped with 12 and 18 MLD cycles (1.4 and 3.4 nm, respectively). Water permeance and NaCl permeability parameters are summarized in Table 3.

Delamination is a major concern for novel RO membranes. However, the MLD-enhanced NF270 membranes showed no sign of delamination throughout all desalination tests. Samples were stable in moderate cross flow conditions (0.13 m/s) for at least 24 h. IP films are formed at the solvent interface whereas MLD films are formed directly on the substrate. Owing to strong covalent bonding between the MLD film and the NF270 layer, MLD-enhanced membranes are expected to evidence long-term mechanical stability that matches that of the substrate NF membrane. Further testing is required to confirm this expectation.

3.3. Effect of precursor infiltration on desalination performance

As an absorbing substrate, the bulk structure of the original NF270 polyamide dense layer could be chemically altered by the MLD precursors. In this process, known as vapor-phase infiltration (VPI), gas-phase reactants enter the substrate film through solution-diffusion and become incorporated into the bulk structure through reactions with previously unreacted functional groups [61].

To test for the effects of VPI within the NF270, exposure times were varied for the MLD reactants. If VPI were to alter the original structure of the dense layer, then desalination performance would be affected both by the top MLD film and by structural modifications via VPI. For increased exposure times, higher rejection and lower permeance metrics would be expected for films with the same MLD film thickness. Testing was performed with exposure times of 0.3, 1.2 and 6 s. Increased exposure time led to increased salt rejection and reduced water permeance for the same number of MLD cycles (Fig. 6a, b). However, as previously noted, higher film growth rates occur with exposure times of 6 s due to the carry-over of absorbed precursors. Therefore, the thickness of the MLD top layer must be considered.

Desalination performance was correlated to thickness of the MLD films for samples with varied exposure times. All exposure times followed a common trend line for NaCl rejection (Fig. 6c) and for water permeance (Fig. 6d). The thickness of the MLD film governed performance while any effects of VPI are not observed. These results indicate that desalination performance is a function of MLD film thickness rather than exposure time, and the tradeoff in desalination performance is attributed to the MLD film grown atop the NF270. Significant VPI effects may occur, but likely require much longer exposure times.

Table 3
Pure water permeance (A) and salt permeability parameters (B) for various membranes and processing conditions. Measurements were performed in a cross flow desalination system with 2000 ppm NaCl feed at 15.5 bar.

Sample	A (L/m^2 h bar)	B (L/m^2 h)
NF270, as-received	22.5 ± 1.2	152 ± 13
NF270 with 0 MLD cycles (heated in vacuum with no chemistry)	12.1 ± 0.8	56 ± 5
NF270 with 12 MLD cycles	2.1 ± 0.2	1.2 ± 0.2
NF270 with 18 MLD cycles	1.4 ± 0.1	0.3 ± 0.2
Toray TMG(D)	1.7 ± 0.2	0.7 ± 0.6

3.4. Temperature effects on desalination performance

MLD modification was performed at a temperature above the manufacturer's maximum operating temperature specification of 45 °C [41]. A processing temperature of 115 °C was required due to the low vapor pressure and subsequently, low flow rate of the TMC precursor [30,62]. Temperature exposure alone did affect membrane performance, as shown by the difference in performance between the as-received and 0-cycles (heated in the vacuum chamber with no chemistry) data in Fig. 4 and confirmed in Figs. S2 and S3. To minimize additional temperature effects, all MLD-processed samples had the same heating time of 11 ± 1 h. As highlighted in Table 4, such temperature exposure caused a decrease in permeance and an increase in rejection. Mänttäri et al. attribute temperature-induced performance difference to a change in membrane morphology and tightening of the membrane structure [63]. Yao et al. ascribe the difference to a reorientation of polymer chains at high temperatures [64]. Moreover, the residence time in the MLD reactor at temperature also had an effect on the performance metrics. NF270 samples that remained in the vacuum chamber for 50 h at 115 °C had a 25% decrease in permeance and a 32% gain in rejection as compared to samples that remained for only 11 ± 1 h. The elevated temperature required and resulting effect on performance represents a current limitation of MLD fabrication.

3.5. Surface characteristics

While no fouling experiments were performed in this initial study of the MLD-modified NF membranes, these membranes possess a number of surface characteristics which offer promise for improved fouling performance. Fouling is often categorized as biofouling, organic, inorganic or colloidal [65]. Many sources suggest that low-roughness, hydrophilic and more neutrally charged surfaces are most desirable to minimize overall fouling [2,66,67]. With respect to hydrophilicity, hydrophobic organic foulants are less inclined to absorb to hydrophilic surfaces [10]. In terms of surface charge, membranes with a neutral charge are desirable to prevent electrostatic interactions with charged foulants although some studies have shown that negatively charged surfaces are effective at repelling negatively charged colloids and bacteria [10,68,69]. Regarding surface roughness, many studies have concluded that the peak and valley morphology of IP films trap colloidal foulants within the valley structures [10,70]. Membranes with lower RMS roughness have been shown to have measurably less colloidal fouling [10,70,71] although other studies dispute this claim [72–74].

The stepwise nature of MLD allows for control over the precursor used for initial and ultimate exposures. A final exposure to MPD would lead to a hydrophilic amine surface. The acyl chloride groups left by a final exposure to TMC hydrolyze into hydrophilic carboxyls upon contact with water. An increased density of carboxyl terminal groups produce a more negative surface charge [68,69]. Thus the final MLD precursor exposure may be useful to affect surface charge.

Contact angle measurements were performed for the MLD membranes. As shown in Fig. 7, all samples placed within the MLD reactor at 115 °C had contact angle values of ~60-70°. This is comparable with other TMC-MPD-based membranes [75]. No significant difference was found between samples terminated with either MPD (amine surface) or TMC (carboxyl surface). These results are similar to those of Werber et al. who found negligible difference in contact angle values for membranes after being quenched in various solutions [76]. Therefore, hydrophilicity of the surface was not significantly affected by the

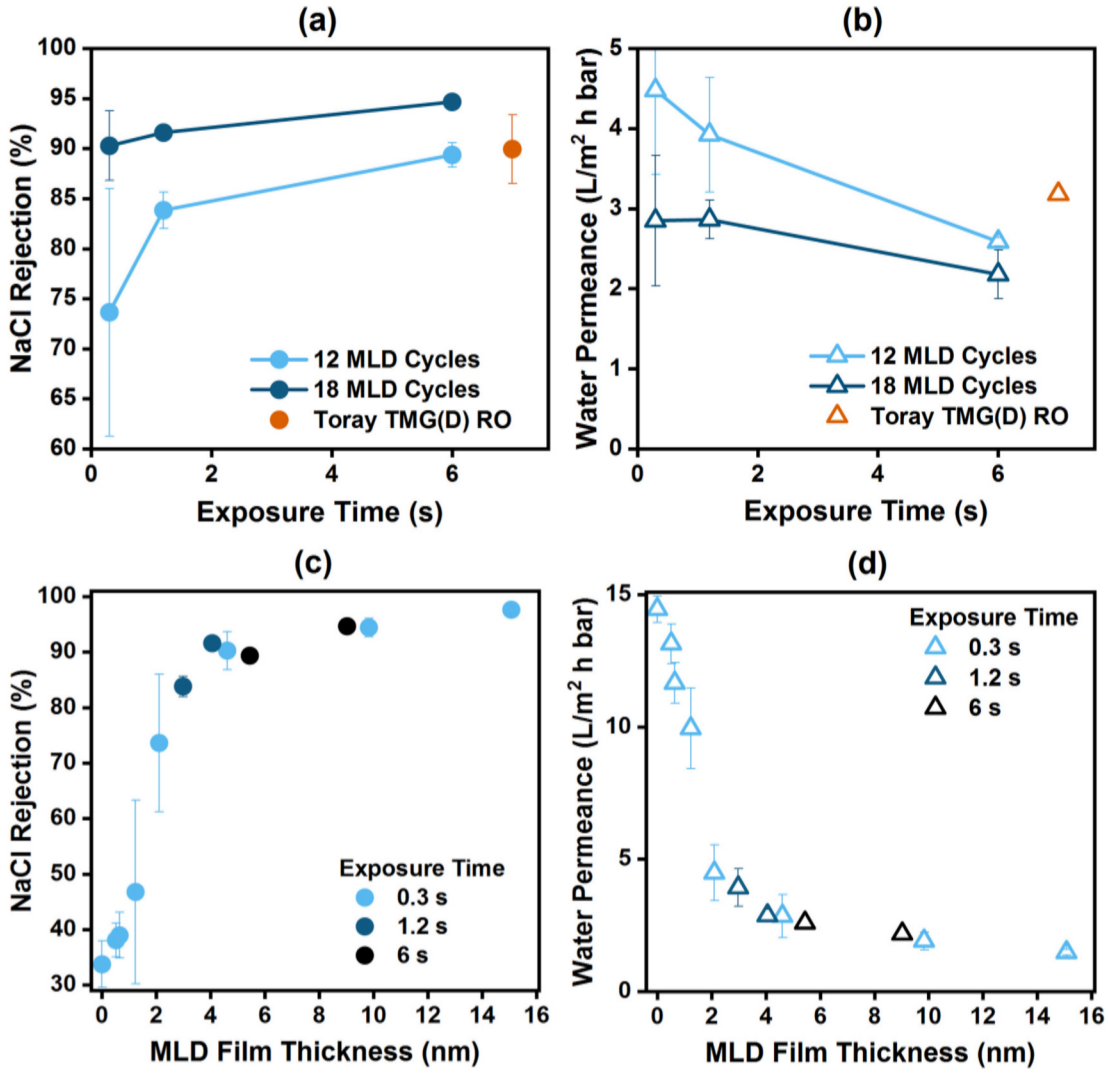

Fig. 6. Desalination performance for MLD membranes grown atop NF270 at precursor exposure times of 0.3, 1.2 and 6 s. (a) NaCl rejection and (b) water permeance are compared to the performance of Toray TMG(D) RO membranes measured using the same dead-end cell procedure. (c) NaCl rejection and (d) water permeance versus film thickness reveal that film thickness governs the tradeoff performance for all tested exposure times.

Table 4
Performance metrics for NF270 membrane samples obtained under different experimental conditions. Measurements were made with the dead-end cell procedure.

Condition	Water permeance (L/m^2 h bar)	NaCl rejection (%)
As-received	20.5 ± 0.9	25 ± 4
Heated in vacuum for 11 h, 115 °C	14.4 ± 0.5	34 ± 4
Heated in vacuum for 50 h, 115 °C	10.8 ± 1.4	45 ± 3
4 MLD cycles, 115 °C	11.7 ± 0.8	39 ± 4
12 MLD cycles, 115 °C	4.5 ± 1.1	74 ± 12
48 MLD cycles, 115 °C	1.5 ± 0.1	98 ± 1

terminal chemistry. However, hydrophilicity was altered by heating alone which is attributed to changes to the molecular structure of the NF270 dense film as suggested by others [63,64].

No appreciable difference in initial desalination performance metrics was observed for the NF270 samples terminated with an exposure to TMC or to MPD (Fig. S4). However, the control over the surface charge would allow for informed engineering of a fouling-resistant surface. The MLD modification process lends itself well to subsequent vacuum processes such as ALD or chemical vapor deposition which have proven effective for enhancement of the membrane surface [77].

AFM was used to investigate the changes in roughness and morphology of the NF270 membrane surface after MLD processing. Fig. 8 shows representative 1 μm × 1 μm 3D images of membrane surfaces before and after the application of 144 MLD cycles (43 nm). Less than 0.1 nm difference in RMS roughness was measured between the 0-cycles sample (heated in the vacuum chamber with no chemistry) and the sample with 144 MLD cycles (Table 5). However, surface roughness features were affected by the MLD film.

The conformal deposition of material by MLD led to a reduction in the lateral spacing of the peaks and valleys, as can be seen in the representative line profiles in Fig. 9. As a result, the small features of the membrane surface, whose lateral spacing was on the order of tens of nanometers, were "filled in" by the 43-nm-thick layer of MLD polyamide. In contrast, larger morphologic features with a greater lateral spacing experienced peak-broadening, but were not removed [78]. This phenomenon is described by Gerritsen who showed that conformal film growth leads to smoothing of small scale features through the broadening of roughness peaks, whereas large-scale roughness features above a critical spacing experience no smoothing [79].

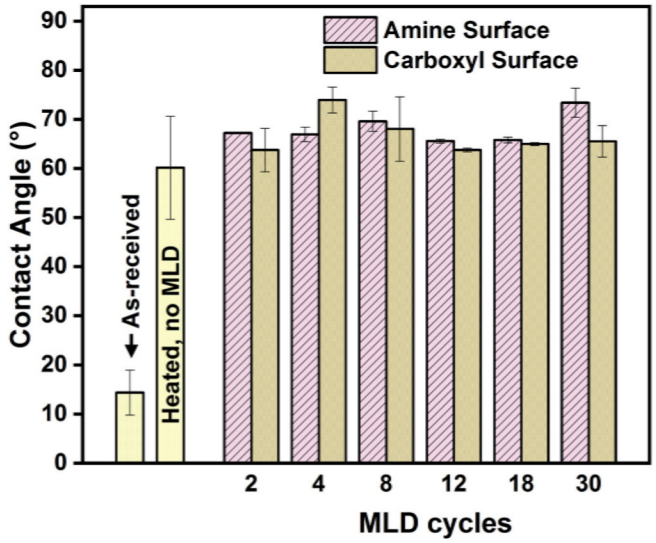

Fig. 7. Contact angles for NF270 membranes topped with MLD films with increasing cycles. Samples were either terminated with MPD (amine surface) or TMC (carboxyl surface) precursors. Results are compared with an as-received NF270 membrane and a NF270 sample which was heated in the vacuum chamber at 115 °C with no chemistry performed.

Effects of MLD smoothing are dependent on the original morphology of the membrane. Although small-scale features in the NF270 were removed by the MLD smoothing effect, RMS roughness remained unchanged. This is attributed to the fact that these features appeared with low frequency. Thus, their original contribution to RMS roughness was negligible. Conversely, asperities with large lateral spacing, namely the "peaks" and "valleys", were dominant. An MLD smoothing effect is expected for other types of membranes whose surfaces contain more instances of small-scale features. Although the ability to control surface features is encouraging, comprehensive studies are required to determine whether and to what extent MLD modification can improve membrane fouling characteristics.

3.6. Molecular layer depositionon other membrane substrates

In addition to the NF270 membranes, MLD films were grown atop HYDRACoRe50 membranes in a similar manner. A comparable MLD-thickness-dependent tradeoff between water permeance and salt rejection was observed for the HYDRACoRe50 samples (Fig. S5). While many commercial NF membranes have a polyamide top layer, the active layer of HYDRACoRe50 membranes is sulfonated polyethersulfone [42]. Successful film growth on the sulfonated polyethersulfone layer demonstrates that MLD enhancement is not limited to polyamide-based materials.

Attempts to directly apply MLD films to porous polyethersulfone ultrafiltration samples (20 nm nominal pore diameters) (MilliporeSigma) were unsuccessful. These attempts resulted in impermeable membranes or samples with negligible salt rejection. This is likely a consequence of the fact that MLD film growth occurs conformally at all surfaces, leading to material deposited on pore walls rather than across pore openings [32].

3.7. Implications and future prospects of molecular layer deposition membranes

This study is the first to demonstrate that MLD is an effective method for creating TFC membranes with performance that compares well to current commercial desalination membranes. The sub-nanometer resolution of MLD led to control over the rejection-permeance tradeoff of the samples. Thus, the technique has great potential in nanofiltration applications where control over multivalent salt selectivity is desirable. The technique also has potential for performance "tuning" in applications such as forward osmosis, pressure retarded RO, dialysis, gas separations and battery separators.

The MLD films were shown have RMS roughness values equal to their underlying membrane substrate while removing nanoscale roughness. The technique could be applied to other surfaces for removal of small-scale roughness. Materials with high instances of such roughness features would likely experience a lowering of RMS roughness values with MLD. Many commercial membranes have surface roughness values an order of magnitude greater than NF270 and are excellent candidates for smoothing by MLD (Table 6).

MLD-based desalination membranes may see commercial application through optimization of this technique. Heating significantly affected the NF270 membranes. If MLD processing can be achieved at near-ambient temperatures, it may prove key in producing membranes with superior tradeoff performance. There is also potential to further improve the rejection-permeance trade-off by utilizing NF membranes with a thinner dense layer and/or a different dense layer composition.

A TFC with a free-standing MLD dense layer atop a porous support

Table 5
Root mean square roughness of the surface of NF270 samples.

NF270 conditions	RMS roughness (nm)
As-received	2.77 ± 0.12
Rinsed and dried	2.63 ± 0.09
0 MLD cycles at 115 °C (heated in vacuum with no chemistry)	2.38 ± 0.07
144 MLD cycles (43 nm) at 115 °C	2.39 ± 0.06

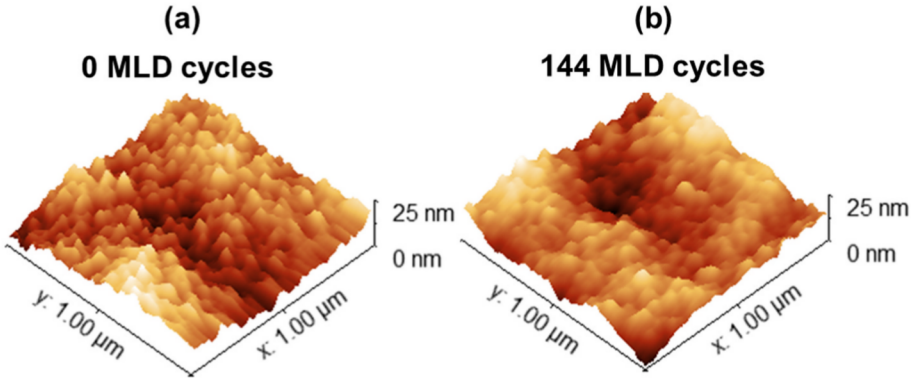

Fig. 8. Representative atomic force microscopy images of NF270 samples. The MLD modification "softened" the morphologic features, but did not affect RMS roughness: (a) NF270 heated in the vacuum chamber with no chemistry; (b) NF270 topped with 144 MLD cycles (43 nm).

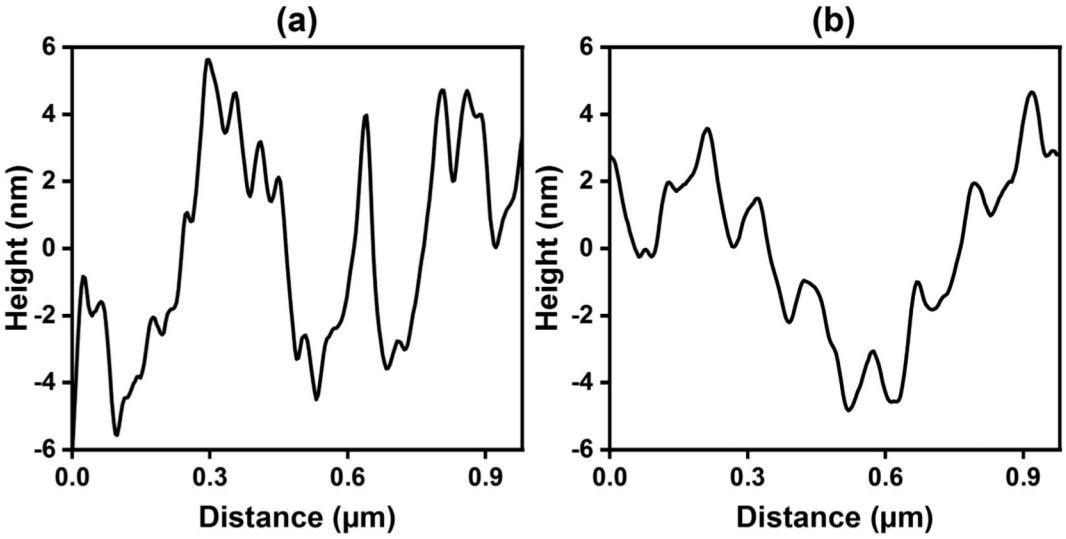

Fig. 9. Atomic force microscopy line profiles of NF270 samples: (a) NF270 heated in the vacuum chamber at 115 °C with no chemistry; (b) NF270 modified with 144 MLD cycles (43 nm).

Table 6
Surface roughness of various commercial NF and RO membranes.

Membrane product	Type	Manufacturer	RMS roughness (nm)	Mean roughness[a] (nm)	Source
NF270	NF	DuPont Filmtec	2.77	11.40	This work & [80]
NF90	NF	DuPont Filmtec	–	124.99	[80]
HYDRACoRe50	NF	Nitto Hydranautics	1.0	–	[81]
ESNA	NF	Nitto Hydranautics	–	29	[82]
TFC-S	NF	Koch		64	[82]
TMG-10	RO	Toray	–	44	[82]
BW30	RO	DuPont Filmtec	38.1	95.52	[75,80]
XLE	RO	DuPont Filmtec	105.8	73, 135.60	[75,80,82]
LFC-1	RO	Nitto Hydranautics	–	70	[83]
LFC-3	RO	Nitto Hydranautics	–	70	[83]
ESPA1	RO	Nitto Hydranautics	–	123	[83]
TFC-HR	RO	Koch	–	64	[82]
TFC-ULP	RO	Koch	–	42	[82]

[a] Method of roughness calculation not specified.

would likely show improved performance characteristics as compared to the MLD-modified NF membranes described here. Ultrathin, ultrasmooth membranes may be possible with the development of an effective fabrication technique. Through covalent bonding directly to a porous support, the MLD dense layer should have excellent mechanical stability and could be applied to high porosity supports for increased separation effectiveness.

The range of conventional IP chemistries are constrained by the IP process itself [14]. Suitable monomer reactants must have the right solubility and reactivity characteristics for IP to succeed. In contrast, MLD is able to deposit a wide range of polymer chemistries including polyureas, polyesters, polyimides, polyamides, polythioureas and polyurethanes [28]. MLD enables the exploration of new semipermeable polymer chemistries and may lead to yet-undiscovered dense film material compositions with superior rejection-permeance tradeoff, fouling resistance and long-term stability.

Furthermore, the MLD process could be used to create nanolaminate films. For example, a TMC-piperazine polyamide layer could be grown in-situ atop the TMC-MPD layer to create a prescreening, nanofiltration nanolayer to affect concentration gradients. By extrapolation, the nanolaminate structure could have a resolution of a single monomer and incorporate a near unlimited range of unique monomers extending beyond the polyamide family. In principle, the monolayer selection possible with MLD is analogous to artificial protein sequencing at small scale. This would enable extreme structural control and the ability to manipulate intrinsic dense layer properties such as density and cross-linking. In effect, unprecedented optimization of the transport of solvents and solutes at the molecular scale would be possible. With such control, it may become viable to engineer membranes which are stable in harsh environments, resistant to ozone and chlorine treatment and/or operable at elevated temperatures and pressures. Thus, the implications extend far beyond desalination membrane applications. Monomer-scale engineering of TFC membranes could lead to further development in other areas of membrane separations.

With future optimization and development of the technique, MLD could become a key component of TFC manufacture. As of this publication, several companies offer R2R web handling equipment capable of applying MLD films to membrane sheets. R2R systems have already been used to apply ALD films in the production of lithium-ion batteries and flexible electronics on a commercial scale, often at atmospheric pressures [84]. Thus, MLD is compatible with existing membrane manufacturing processes.

4. Conclusions

Molecular layer deposition is an attractive synthesis technique for membrane applications owing to its ability to create conformal, smooth, compositionally controlled polymer films with molecular precision

[27,32]. This work demonstrated that desalination membranes with tailor-made perm-selectivity can be achieved by enhancing NF membranes with MLD. FilmTec NF270 nanofiltration membranes were modified with MLD via application of an aromatic polyamide thin-film from the gas-phase polymerization of trimesoyl chloride and *m*-phenylenediamine. In particular, the number of MLD cycles and the exposure time for each reactant were carefully controlled. The initial performance metrics of the resulting TFC membranes were evaluated in a stirred, dead-end cell and in a cross flow system.

High salt-rejection membranes could be fabricated with this technique. Membranes fabricated with a greater number of MLD cycles evidenced improved salt rejection but decreased water permeance. In comparison with a small sample of commercial membranes, MLD-modified membranes with a 5 nm thin-film evidenced generally equivalent salt rejection values whereas those with a $>$ 5 nm thin-film exceeded the benchmark. Precursor infiltration effects were studied by increasing exposure time to each MLD reactant per cycle from 0.3 to 6 s. The trend in desalination performance according to MLD film thickness remained unchanged regardless of exposure time.

In addition to the NF270 membranes, HYDRACoRe50 membranes were modified with MLD in a similar manner whereby a comparable MLD-thickness-dependent tradeoff between water permeance and salt rejection was observed. Successful enhancement of the NF polyethersulfone layer demonstrates that MLD application is not limited to polyamide-based materials.

Atomic force microscopy measurements revealed that MLD modification of the NF270 membranes led to the smoothing of small morphologic features. The RMS roughness, however, was unaffected. In combination, the ability of MLD to control terminal surface chemistry as well as surface morphology may provide a route for improved fouling behavior.

CRediT authorship contribution statement

Brian C. Welch: Conceptualization, Methodology, Software, Formal Analysis, Investigation, Writing – Original Draft, Writing – Review & Editing, Visualization

Olivia M. McIntee: Validation, Investigation, Writing – Review & Editing

Tyler J. Myers: Formal Analysis, Investigation, Visualization

Alan R. Greenberg: Conceptualization, Writing – Review & Editing, Supervision, Funding Acquisition

Victor M. Bright: Writing – Review & Editing, Supervision, Funding Acquisition

Steven M. George: Conceptualization, Funding Acquisition

Declaration of competing interest

The authors declare that they have no known competing financial interests or personal relationships that could have appeared to influence the work reported in this paper.

Acknowledgements

This research was supported by the National Science Foundation (NSF) through the "Membrane Science, Engineering and Technology Center" [NSF IUCRC Award IIP 1624602] at the University of Colorado, Boulder. The authors thank James Redmond, Eliot Fang and John Emery of Sandia National Laboratories, Christina Carbrello of MilliporeSigma and Sankaranarayanan Ravichandran of the University of Colorado for helpful technical discussions. Special thanks to Prof. Anthony Straub of the University of Colorado for equipment-sharing and insightful collaboration. In addition, the authors thank DuPont Filmtec and Nitto Hydranautics for supplying membrane samples.

Appendix A. Supplementary material

Supplementary material to this article can be found online at https://doi.org/10.1016/j.desal.2021.115334.

References

[1] S. Karan, Z. Jiang, A.G. Livingston, Sub–10 nm polyamide nanofilms with ultrafast solvent transport for molecular separation, Science 348 (2015) 1347–1351, https://doi.org/10.1126/science.aaa5058.

[2] J.R. Werber, C.O. Osuji, M. Elimelech, Materials for next-generation desalination and water purification membranes, Nat. Rev. Mater. 1 (2016) 1–15, https://doi.org/10.1038/natrevmats.2016.18.

[3] P.S. Singh, S.V. Joshi, J.J. Trivedi, C.V. Devmurari, A.P. Rao, P.K. Ghosh, Probing the structural variations of thin film composite RO membranes obtained by coating polyamide over polysulfone membranes of different pore dimensions, J. Membr. Sci. 278 (2006) 19–25, https://doi.org/10.1016/j.memsci.2005.10.039.

[4] A.K. Ghosh, E.M.V. Hoek, Impacts of support membrane structure and chemistry on polyamide–polysulfone interfacial composite membranes, J. Membr. Sci. 336 (2009) 140–148, https://doi.org/10.1016/j.memsci.2009.03.024.

[5] S.-J. Park, W. Choi, S.-E. Nam, S. Hong, J.S. Lee, J.-H. Lee, Fabrication of polyamide thin film composite reverse osmosis membranes via support-free interfacial polymerization, J. Membr. Sci. 526 (2017) 52–59, https://doi.org/10.1016/j.memsci.2016.12.027.

[6] R.H. Hailemariam, Y.C. Woo, M.M. Damtie, B.C. Kim, K.-D. Park, J.-S. Choi, Reverse osmosis membrane fabrication and modification technologies and future trends: a review, Adv. Colloid Interface Sci. 276 (2020), 102100, https://doi.org/10.1016/j.cis.2019.102100.

[7] S. Habib, S.T. Weinman, A review on the synthesis of fully aromatic polyamide reverse osmosis membranes, Desalination 502 (2021), 114939, https://doi.org/10.1016/j.desal.2021.114939.

[8] T.E. Culp, B. Khara, K.P. Brickey, M. Geitner, T.J. Zimudzi, J.D. Wilbur, S.D. Jons, A. Roy, M. Paul, B. Ganapathysubramanian, A.L. Zydney, M. Kumar, E.D. Gomez, Nanoscale control of internal inhomogeneity enhances water transport in desalination membranes, Science 371 (2021) 72–75, https://doi.org/10.1126/science.abb8518.

[9] Z. Jiang, S. Karan, A.G. Livingston, Water transport through ultrathin polyamide nanofilms used for reverse osmosis, Adv. Mater. 30 (2018), 1705973, https://doi.org/10.1002/adma.201705973.

[10] S. Zhao, Z. Liao, A. Fane, J. Li, C. Tang, C. Zheng, J. Lin, L. Kong, Engineering antifouling reverse osmosis membranes: a review, Desalination 499 (2021), 114857, https://doi.org/10.1016/j.desal.2020.114857.

[11] P.M. Johnson, J. Yoon, J.Y. Kelly, J.A. Howarter, C.M. Stafford, Molecular layer-by-layer deposition of highly crosslinked polyamide films, J. Polym. Sci. B Polym. Phys. 50 (2012) 168–173, https://doi.org/10.1002/polb.23002.

[12] H. Qian, S. Li, J. Zheng, S. Zhang, Ultrathin films of organic networks as nanofiltration membranes via solution-based molecular layer deposition, Langmuir 28 (2012) 17803–17810, https://doi.org/10.1021/la304196q.

[13] J.-E. Gu, S. Lee, C.M. Stafford, J.S. Lee, W. Choi, B.-Y. Kim, K.-Y. Baek, E.P. Chan, J. Y. Chung, J. Bang, J.-H. Lee, Molecular layer-by-layer assembled thin-film composite membranes for water desalination, Adv. Mater. 25 (2013) 4778–4782, https://doi.org/10.1002/adma.201302030.

[14] W. Choi, J.-E. Gu, S.-H. Park, S. Kim, J. Bang, K.-Y. Baek, B. Park, J.S. Lee, E. P. Chan, J.-H. Lee, Tailor-made polyamide membranes for water desalination, ACS Nano 9 (2015) 345–355, https://doi.org/10.1021/nn505318v.

[15] X. Song, S. Qi, C.Y. Tang, C. Gao, Ultra-thin, multi-layered polyamide membranes: synthesis and characterization, J. Membr. Sci. 540 (2017) 10–18, https://doi.org/10.1016/j.memsci.2017.06.016.

[16] W.D. Mulhearn, V.P. Oleshko, C.M. Stafford, Thickness-dependent permeance of molecular layer-by-layer polyamide membranes, J. Membr. Sci. 618 (2021), 118637, https://doi.org/10.1016/j.memsci.2020.118637.

[17] M.R. Chowdhury, J. Steffes, B.D. Huey, J.R. McCutcheon, 3D printed polyamide membranes for desalination, Science 361 (2018) 682–686, https://doi.org/10.1126/science.aar2122.

[18] S.-B. Kwon, J.S. Lee, S.J. Kwon, S.-T. Yun, S. Lee, J.-H. Lee, Molecular layer-by-layer assembled forward osmosis membranes, J. Membr. Sci. 488 (2015) 111–120, https://doi.org/10.1016/j.memsci.2015.04.015.

[19] H. Zhou, S.F. Bent, Fabrication of organic interfacial layers by molecular layer deposition: present status and future opportunities, J. Vac. Sci. Technol. A 31 (2013), 040801, https://doi.org/10.1116/1.4804609.

[20] S.M. George, B. Yoon, A.A. Dameron, Surface chemistry for molecular layer deposition of organic and hybrid organic-inorganic polymers, Acc. Chem. Res. 42 (2009) 498–508, https://doi.org/10.1021/ar800105q.

[21] J. Sheng, J.-H. Lee, W.-H. Choi, T. Hong, M. Kim, J.-S. Park, Review article: atomic layer deposition for oxide semiconductor thin film transistors: advances in research and development, J. Vac. Sci. Technol. A 36 (2018), 060801, https://doi.org/10.1116/1.5047237.

[22] M. Junige, S.M. George, Area-selective molecular layer deposition of nylon 6,2 polyamide: growth on carbon and inhibition on silica, J. Vac. Sci. Technol. A 39 (2021), 023204, https://doi.org/10.1116/6.0000769.

[23] n/a-n/a C. Ban, S.M. George, Molecular layer deposition for surface modification of lithium-ion battery electrodes, Adv. Mater. Interfaces 3 (2016), https://doi.org/10.1002/admi.201600762.

[24] Y. Zhao, L. Zhang, J. Liu, K. Adair, F. Zhao, Y. Sun, T. Wu, X. Bi, K. Amine, J. Lu, X. Sun, Atomic/molecular layer deposition for energy storage and conversion, Chem. Soc. Rev. (2021), https://doi.org/10.1039/D0CS00156B.
[25] J. Bachmann, Atomic Layer Deposition in Energy Conversion Applications, John Wiley & Sons, 2017.
[26] M. Weber, A. Julbe, A. Ayral, P. Miele, M. Bechelany, Atomic layer deposition for membranes: basics, challenges, and opportunities, Chem. Mater. 30 (2018) 7368–7390, https://doi.org/10.1021/acs.chemmater.8b02687.
[27] H. Zhou, M.F. Toney, S.F. Bent, Cross-linked ultrathin polyurea films via molecular layer deposition, Macromolecules 46 (2013) 5638–5643, https://doi.org/10.1021/ma400998m.
[28] X. Meng, An overview of molecular layer deposition for organic and organic–inorganic hybrid materials: mechanisms, growth characteristics, and promising applications, J. Mater. Chem. A 5 (2017) 18326–18378, https://doi.org/10.1039/C7TA04449F.
[29] Y. Du, S.M. George, Molecular layer deposition of nylon 66 films examined using in situ FTIR spectroscopy, J. Phys. Chem. C 111 (2007) 8509–8517, https://doi.org/10.1021/jp067041n.
[30] D.J. Higgs, J.W. DuMont, K. Sharma, S.M. George, Spatial molecular layer deposition of polyamide thin films on flexible polymer substrates using a rotating cylinder reactor, J. Vac. Sci. Technol. A 36 (2017) 01A117, https://doi.org/10.1116/1.5004041.
[31] J.M. Wallas, B.C. Welch, Y. Wang, J. Liu, S.E. Hafner, R. Qiao, T. Yoon, Y.-T. Cheng, S.M. George, C. Ban, Spatial molecular layer deposition of ultrathin polyamide to stabilize silicon anodes in lithium-ion batteries, ACS Appl. Energy Mater. 2 (2019) 4135–4143, https://doi.org/10.1021/acsaem.9b00326.
[32] B.C. Welch, O.M. McIntee, A.B. Ode, B.B. McKenzie, A.R. Greenberg, V.M. Bright, S.M. George, Continuous polymer films deposited on top of porous substrates using plasma-enhanced atomic layer deposition and molecular layer deposition, J. Vac. Sci. Technol. A 38 (2020), 052409, https://doi.org/10.1116/6.0000271.
[33] A.S. Yersak, Y.C. Lee, J.A. Spencer, M.D. Groner, Atmospheric pressure spatial atomic layer deposition web coating with in situ monitoring of film thickness, J. Vac. Sci. Technol. A 32 (2013) 01A130, https://doi.org/10.1116/1.4850176.
[34] C.-H. Chao, C.-T. Hsieh, W.-J. Ke, L.-W. Lee, Y.-F. Lin, H.-W. Liu, S. Gu, C.-C. Fu, R.-S. Juang, B.C. Mallick, Y.A. Gandomi, C.-Y. Su, Roll-to-roll atomic layer deposition of titania coating on polymeric separators for lithium ion batteries, J. Power Sources 482 (2021), 228896, https://doi.org/10.1016/j.jpowsour.2020.228896.
[35] G. Artug, I. Roosmasari, K. Richau, J. Hapke, A comprehensive characterization of commercial nanofiltration membranes, Sep. Sci. Technol. 42 (2007) 2947–2986, https://doi.org/10.1080/01496390701560082.
[36] J. Black, G. Hastings (Eds.), Handbook of Biomaterial Properties, Springer, US, 1998, https://doi.org/10.1007/978-1-4615-5801-9.
[37] FILMTECTM Membranes Product Information Catalog, Dow Water Solutions, n.d.
[38] L. Puro, M. Mänttäri, A. Pihlajamäki, M. Nyström, Characterization of modified nanofiltration membranes by octanoic acid permeation and FTIR analysis, Chem. Eng. Res. Des. 84 (2006) 87–96, https://doi.org/10.1205/cherd.04036.
[39] V. Freger, J. Gilron, S. Belfer, TFC polyamide membranes modified by grafting of hydrophilic polymers: an FT-IR/AFM/TEM study, J. Membr. Sci. 209 (2002) 283–292, https://doi.org/10.1016/S0376-7388(02)00356-3.
[40] K. Boussu, Y. Zhang, J. Cocquyt, P. Van der Meeren, A. Volodin, C. Van Haesendonck, J.A. Martens, B. Van der Bruggen, Characterization of polymeric nanofiltration membranes for systematic analysis of membrane performance, J. Membr. Sci. 278 (2006) 418–427, https://doi.org/10.1016/j.memsci.2005.11.027.
[41] FilmTecTM NF270 Nanofiltration Elements for Commercial Systems, DuPont Water Solutions, n.d.
[42] HYDRACoRe10 and 50 LD Series Datasheet, Hydranautics, n.d.
[43] FILMTECTM Reverse Osmosis Membranes Technical Manual, Dow Water Solutions, n.d.
[44] Toray TMG(D) Datasheet, Toray Industries Inc, n.d.
[45] FilmTec BW30HRLE-440 Element Datasheet, DuPont, n.d.
[46] Flat Sheet Membrane Chart, Suez, n.d.
[47] K. Sharma, R.A. Hall, S.M. George, Spatial atomic layer deposition on flexible substrates using a modular rotating cylinder reactor, J. Vac. Sci. Technol. A 33 (2015) 01A132, https://doi.org/10.1116/1.4902086.
[48] K. Sharma, D. Routkevitch, N. Varaksa, S.M. George, Spatial atomic layer deposition on flexible porous substrates: ZnO on anodic aluminum oxide films and Al2O3 on Li ion battery electrodes, J. Vac. Sci. Technol. A 34 (2016), 01A146, https://doi.org/10.1116/1.4937728.
[49] A.S. Yersak, K. Sharma, J.M. Wallas, A.A. Dameron, X. Li, Y. Yang, K.E. Hurst, C. Ban, R.C. Tenent, S.M. George, Spatial atomic layer deposition for coating flexible porous Li-ion battery electrodes, J. Vac. Sci. Technol. A 36 (2017), 01A123, https://doi.org/10.1116/1.5006670.
[50] FiveEasy PlusTM Conductivity Meter FP30 Operation Instructions, Mettler Toledo, 2020.
[51] T. Tsuru, S. Sasaki, T. Kamada, T. Shintani, T. Ohara, H. Nagasawa, K. Nishida, M. Kanezashi, T. Yoshioka, Multilayered polyamide membranes by spray-assisted 2-step interfacial polymerization for increased performance of trimesoyl chloride (TMC)/m-phenylenediamine (MPD)-derived polyamide membranes, J. Membr. Sci. 446 (2013) 504–512, https://doi.org/10.1016/j.memsci.2013.07.031.
[52] R.A. Robinson, The vapour pressures of solutions of potassium chloride and sodium chloride, Trans. Proc. R. Soc. N. Z. 75 (1945) 203–217.
[53] S.R. Yadhuraj, G. Satheesh Babu, M. Uttara Kumari, Measurement of thickness and roughness using gwyddion, in: 2016 3rd International Conference on Advanced Computing and Communication Systems (ICACCS), 2016, pp. 1–5, https://doi.org/10.1109/ICACCS.2016.7586314.
[54] J.D. Ferguson, A.W. Weimer, S.M. George, Atomic layer deposition of Al2O3 films on polyethylene particles, Chem. Mater. 16 (2004) 5602–5609, https://doi.org/10.1021/cm040008y.
[55] G.M. Geise, H.B. Park, A.C. Sagle, B.D. Freeman, J.E. McGrath, Water permeability and water/salt selectivity tradeoff in polymers for desalination, J. Membr. Sci. 369 (2011) 130–138, https://doi.org/10.1016/j.memsci.2010.11.054.
[56] S. Chaudhury, E. Wormser, Y. Harari, E. Edri, O. Nir, Tuning the ion-selectivity of thin-film composite nanofiltration membranes by molecular layer deposition of alucone, ACS Appl. Mater. Interfaces (2020), https://doi.org/10.1021/acsami.0c16569.
[57] S.M. George, Atomic layer deposition: an overview, Chem. Rev. 110 (2010) 111–131, https://doi.org/10.1021/cr900056b.
[58] J.R. Werber, A. Deshmukh, M. Elimelech, The critical need for increased selectivity, not increased water permeability, for desalination membranes, Environ. Sci. Technol. Lett. 3 (2016) 112–120, https://doi.org/10.1021/acs.estlett.6b00050.
[59] D. Cohen-Tanugi, R.K. McGovern, S.H. Dave, J.H. Lienhard, J.C. Grossman, Quantifying the potential of ultra-permeable membranes for water desalination, Energy Environ. Sci. 7 (2014) 1134–1141, https://doi.org/10.1039/C3EE43221A.
[60] A. Deshmukh, N.Y. Yip, S. Lin, M. Elimelech, Desalination by forward osmosis: identifying performance limiting parameters through module-scale modeling, J. Membr. Sci. 491 (2015) 159–167, https://doi.org/10.1016/j.memsci.2015.03.080.
[61] A. Sinha, D.W. Hess, C.L. Henderson, Transport behavior of atomic layer deposition precursors through polymer masking layers: influence on area selective atomic layer deposition, J. Vacuum Sci. Technol. B Microelectron. Nanometer Struct. Process. Meas. Phenom. 25 (2007) 1721–1728, https://doi.org/10.1116/1.2782546.
[62] P. Sundberg, M. Karppinen, Organic and inorganic-organic thin film structures by molecular layer deposition: a review, Beilstein J. Nanotechnol. 5 (2014) 1104–1136, https://doi.org/10.3762/bjnano.5.123.
[63] M. Mänttäri, A. Pihlajamäki, E. Kaipainen, M. Nyström, Effect of temperature and membrane pre-treatment by pressure on the filtration properties of nanofiltration membranes, Desalination 145 (2002) 81–86, https://doi.org/10.1016/S0011-9164(02)00390-9.
[64] W.X. Yao, K.J. Kennedy, C.M. Tam, J.D. Hazlett, Pre-treatment of Kraft pulp bleach plant effluent by selected ultrafiltration membranes, Can. J. Chem. Eng. 72 (1994) 991–999, https://doi.org/10.1002/cjce.5450720608.
[65] S. Jiang, Y. Li, B.P. Ladewig, A review of reverse osmosis membrane fouling and control strategies, Sci. Total Environ. 595 (2017) 567–583, https://doi.org/10.1016/j.scitotenv.2017.03.235.
[66] M. Mulder, Basic Principles of Membrane Technology, 2nd ed., Springer, Netherlands, 1996 https://doi.org/10.1007/978-94-009-1766-8.
[67] D. Li, H. Wang, Recent developments in reverse osmosis desalination membranes, J. Mater. Chem. 20 (2010) 4551–4566, https://doi.org/10.1039/B924553G.
[68] C.Y. Tang, Y.-N. Kwon, J.O. Leckie, Probing the nano- and micro-scales of reverse osmosis membranes—a comprehensive characterization of physiochemical properties of uncoated and coated membranes by XPS, TEM, ATR-FTIR, and streaming potential measurements, J. Membr. Sci. 287 (2007) 146–156, https://doi.org/10.1016/j.memsci.2006.10.038.
[69] C.R. Bartels, M. Wilf, K. Andes, J. Iong, Design considerations for wastewater treatment by reverse osmosis, Water Sci. Technol. 51 (2005) 473–482, https://doi.org/10.2166/wst.2005.0670.
[70] E.M. Vrijenhoek, S. Hong, M. Elimelech, Influence of membrane surface properties on initial rate of colloidal fouling of reverse osmosis and nanofiltration membranes, J. Membr. Sci. 188 (2001) 115–128, https://doi.org/10.1016/S0376-7388(01)00376-3.
[71] C. Hobbs, J. Taylor, S. Hong, Effect of surface roughness on fouling of RO and NF membranes during filtration of a high organic surficial groundwater, J. Water Supply Res. Technol. Aqua 55 (2006) 559–570, https://doi.org/10.2166/aqua.2006.038.
[72] X. Yan, G. Liu, M. Dickey, C.G. Willson, Preparation of porous polymer membranes using nano- or micro-pillar arrays as templates, Polymer 45 (2004) 8469–8474, https://doi.org/10.1016/j.polymer.2004.09.073.
[73] Y. Ding, S. Maruf, M. Aghajani, A.R. Greenberg, Surface patterning of polymeric membranes and its effect on antifouling characteristics, Sep. Sci. Technol. 52 (2017) 240–257, https://doi.org/10.1080/01496395.2016.1201115.
[74] Z. Jiang, S. Karan, A.G. Livingston, Membrane fouling: does microscale roughness matter? Ind. Eng. Chem. Res. 59 (2020) 5424–5431, https://doi.org/10.1021/acs.iecr.9b04798.
[75] Y. Fang, S.J. Duranceau, Study of the effect of nanoparticles and surface morphology on reverse osmosis and nanofiltration membrane productivity, Membranes 3 (2013) 196–225, https://doi.org/10.3390/membranes3030196.
[76] J.R. Werber, S.K. Bull, M. Elimelech, Acyl-chloride quenching following interfacial polymerization to modulate the water permeability, selectivity, and surface charge of desalination membranes, J. Membr. Sci. 535 (2017) 357–364, https://doi.org/10.1016/j.memsci.2017.04.041.
[77] M.O. Mavukkandy, S.A. McBride, D.M. Warsinger, N. Dizge, S.W. Hasan, H. A. Arafat, Thin film deposition techniques for polymeric membranes– a review, J. Membr. Sci. (2020), 118258, https://doi.org/10.1016/j.memsci.2020.118258.
[78] T.J. Myers, J.A. Throckmorton, R.A. Borrelli, M. O'Sullivan, T. Hatwar, S. M. George, Smoothing surface roughness using Al2O3 atomic layer deposition, Appl. Surf. Sci. (2021), 150878, https://doi.org/10.1016/j.apsusc.2021.150878.
[79] S. Gerritsen, Surface Smoothing Using Atomic Layer Deposition and Etching, Eindhoven University of Technology, 2020. Student thesis: Master.

[80] B.M. Xaba, S.J. Modise, B.J. Okoli, M.E. Monapathi, S. Nelana, Characterization of selected polymeric membranes used in the separation and recovery of palladium-based catalyst systems, Membranes (Basel) 10 (2020) 166, https://doi.org/10.3390/membranes10080166.

[81] C.M. Schmidt, M. Sprunk, R. Löffler, J. Hinrichs, Relating nanofiltration membrane morphology to observed rejection of saccharides, Sep. Purif. Technol. 239 (2020), 116550, https://doi.org/10.1016/j.seppur.2020.116550.

[82] P. Xu, J.E. Drewes, Viability of nanofiltration and ultra-low pressure reverse osmosis membranes for multi-beneficial use of methane produced water, Sep. Purif. Technol. 52 (2006) 67–76, https://doi.org/10.1016/j.seppur.2006.03.019.

[83] Q. Li, Z. Xu, I. Pinnau, Fouling of reverse osmosis membranes by biopolymers in wastewater secondary effluent: role of membrane surface properties and initial permeate flux, J. Membr. Sci. 290 (2007) 173–181, https://doi.org/10.1016/j.memsci.2006.12.027.

[84] T.O. Kääriäinen, Roll-to-roll ALD for Lithium-ion Batteries, 2020. https://www.forgenano.com/pald-summit/pald-tools-and-techniques-roll-to-roll-ald-for-lithium-ion-batteries/. (Accessed 10 August 2021).